THE JOURNAL OF PHYSICAL CHEMISTRY C

Article

pubs.acs.org/JPCC

Efficient Förster Resonance Energy Transfer Donors of In(Zn)P/ZnS Quantum Dots

Yemliha Altıntas,[†] Mohammad Younis Talpur,[‡] and Evren Mutlugün*[,‡]

[†]Department of Materials Science and Nanotechnology, Abdullah Gül University, Kayseri TR-38080, Turkey

[‡]Department of Electrical-Electronics Engineering, Abdullah Gül University, Kayseri TR-38080, Turkey

Supporting Information

ABSTRACT: We demonstrate a detailed investigation of the effect of the type and concentration of zinc precursor on the optical properties of In(Zn)P/ZnS quantum dots. We achieved up to 87% quantum yield along with 54 nm emission bandwidth for the green emitters with changing the concentration of the Zn precursors. Employing efficient green emitters as the donor species, we demonstrated an efficient Förster resonance energy transfer (FRET) couple of green and red emitting InP-based quantum dots. With a FRET efficiency level of 70.3% achieved (analyzed from the donor lifetime with and without an acceptor), we further demonstrated the enhancement of the acceptor emission nearly twofold due to the energy transfer. Our results provide new insights toward the understanding of the excitonic interactions among donor and acceptor quantum dots of the III−V family for light harvesting applications.

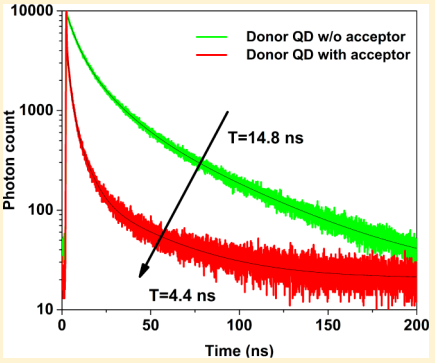

INTRODUCTION

Having been a candidate for the billion United States dollar market by 2020,[1] colloidal quantum dots (QDs) have been the focus of research in optoelectronics. Along with their exotic optical features, they offer innovative applications for lighting and displays. Because the composition of QDs have an important aspect for environmental concerns, the primarily used QDs of the CdSe family are starting to be challenged by InP-based QDs with advances in their synthetic chemistry. Although the potential of the InP-based QDs has been hindered due to associated trap states, which is a common nature of the III−V material systems. Recently, the efforts on InP-based QDs have succeeded in providing high quantum yield particles along with narrow full width at half-maximum (fwhm) values.[2]

The effect of the individual precursors and their type and ratio with the other precursors used in the synthesis has a huge impact on determining the optical properties of the QDs and achieving the desired tunability in their emission character. In that regard, the study of the effect of chain length,[3] the role of the sulfur precursor,[4] and the investigation of the ratio of the indium to phosphor precursor and ligands[5] have all been investigated previously to enhance the photoluminescence quantum yield. Recently, changing the carboxylate ligands with the phosphine ligands has been demonstrated to control the reactivity of the phosphor precursor during the nucleation phase to possess narrow emission bandwidths.[6] Ramasamy et al. reported the influence of trace amounts of water to enhance the quality of synthesized InP/ZnS.[7] As an important step toward the investigation of single molecular precursors, thiocarbamates have been shown to enhance the optical properties of the synthesized In(Zn)P/ZnS.[8] Suppression of the nonradiative and sub band gap transitions by incorporating Zn into phosphate layer has been investigated by Xi et al.[9] In their work, they showed that the ratio of 0.5 to 1 for Zn undecylenate to In gave the highest quantum yield, above 50% for the particles emitting in the red spectral region.

Apart from the high quantum yield, the emission bandwidth also has a huge impact on the performance evaluation of the quantum dots.[10] The narrow fwhm reduces the crosstalk between emitters and provides pure emission characteristics for display applications. With advances in their size distributions, InP-based QDs have started to emerge in monochromatic electroluminescent devices, i.e., QLEDs.[11,12]

In addition to the physical processes involved, the purity of the emitters is also important to make them efficient candidates for energy transfer applications. Also known as the nonradiative energy transfer, Förster resonance energy transfer (FRET) is the energy transfer between donor and acceptor pairs in proximity based on dipole−dipole interaction. In this sort of arrangement, some critical requirements must be met to generate an efficient FRETing medium. The spectral overlap of the donor emission spectrum with the absorption spectra of the acceptor and the high quantum yield of the donor both are the factors enhancing the efficiency of the energy transfer. Quantum dots have been used efficiently as energy transferring donors in recent years.[13,14] In that aspect, one of the important characters of the donor species is that there should be minimal overlap between the donor and acceptor emission spectrum. Otherwise, the overlap of the donor emission and acceptor

Received: October 4, 2016
Revised: January 1, 2017
Published: January 3, 2017

DOI: 10.1021/acs.jpcc.6b09978
J. Phys. Chem. C 2017, 121, 3034−3043

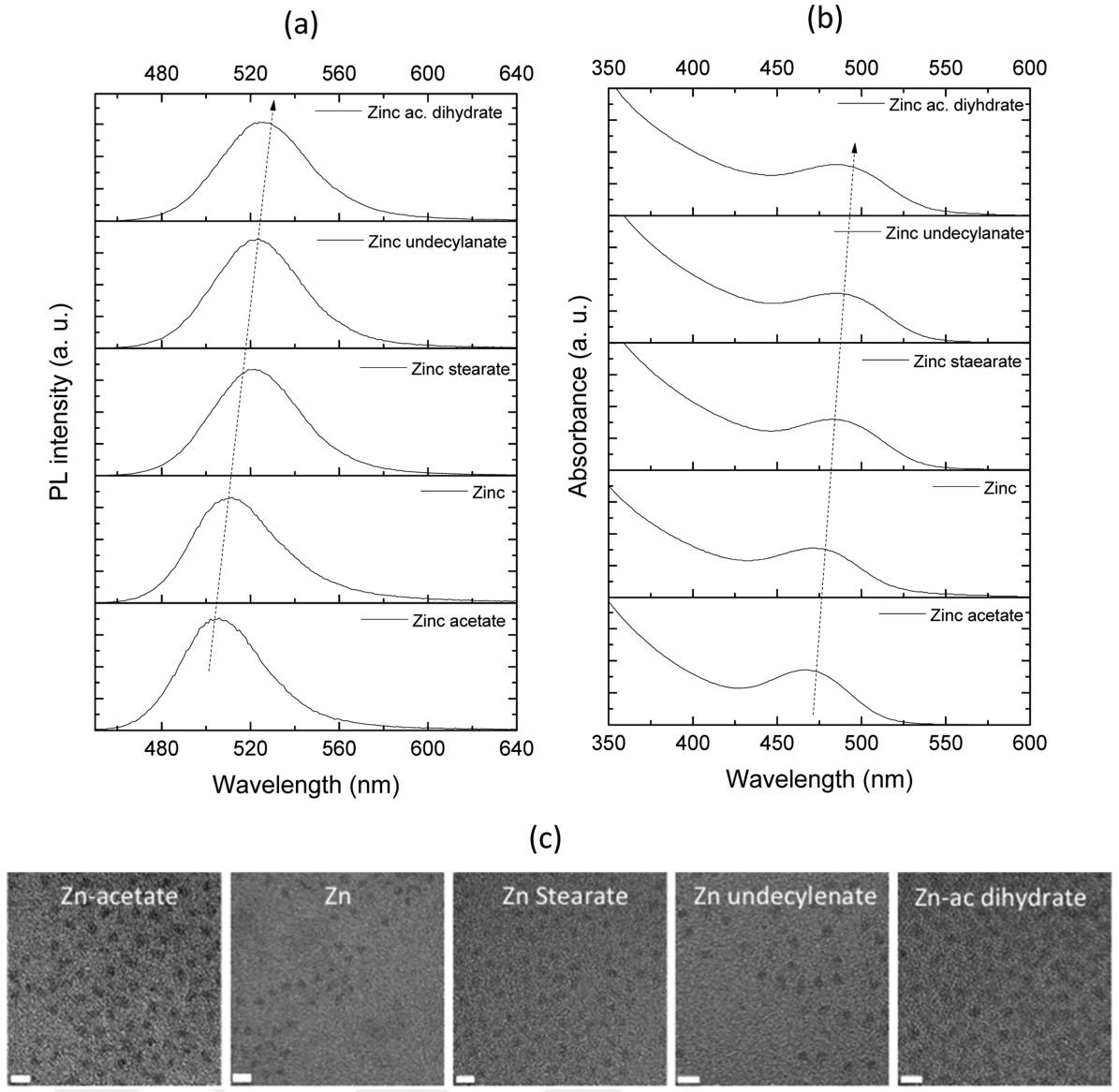

Figure 1. (a) Photoluminescence spectrum, (b) absorption spectrum, and (c) high-resolution transmission electron microscopy (HR-TEM) image (scale bar is 5 nm) for In(Zn)P/ZnS QDs using different Zn precursors.

emission prevents the possibility of safe analysis of the emission kinetics and misleads the interpretation. Recently, the potential of the InP QDs as FRET donors was demonstrated by Thomas et al.[15] The recent review by Guzelturk et al. highlights the importance of utilization of nonradiative energy transfer for the realization of excitonic optoelectronic devices and applications.[16]

RESULTS AND DISCUSSION

Within this context, we focused on the study of the synthesis of In(Zn)P/ZnS QDs via an in-depth investigation of their potential as energy transfer pairs. We extensively studied the effect of Zn precursor type and ratio for achieving high quantum yield particles along with narrow emission bandwidth for the green emitting donor In(Zn)P/ZnS QDs. For the acceptor species, red emitting InP/ZnS QDs were synthesized, and we tuned the emission peak by changing the P precursor concentration used in the synthesis. Upon achieving the high quantum yield particles with narrow emission bandwidth, we incorporated them into a polymer matrix and studied the nonradiative energy transfer among them by carefully adjusting their individual ratio to each other. We demonstrated green emitting In(Zn)P/ZnS at a peak emission wavelength of 525 nm with 81% quantum yield along with 55 nm fwhm as the donor species and 624 nm emitting red QDs with 43% quantum yield and 56 nm fwhm in our report. The QDs were further blended with a polymer matrix, and the emission kinetics upon FRET was extensively studied.

To understand the effect of the Zn precursor on the optical properties of the QDs, we used elemental Zn, Zn stearate, Zn acetate, Zn acetate dihydrate, and Zn undecylenate as the Zn precursors. Figures 1a and b show the evolution of the absorption and photoluminescence spectra of In(Zn)P/ZnS, of which the type of Zn precursor was varied both for the alloyed core growth stage and after the shell coating. Figure 1c shows the high-resolution transmission electron microscopy (TEM) image of the In(Zn)P/ZnS synthesized with different Zn precursors. The change in the peak emission wavelength of the colloidal quantum dots has been attributed to the change in

DOI: 10.1021/acs.jpcc.6b09978
J. Phys. Chem. C 2017, 121, 3034−3043

their electronic energy levels rather than a significant change in their physical sizes. In this set of synthesis work, we used the modified method outlined in the literature.[4,5,17] The details of the synthesis method are presented in the Methods section. It has been shown that using elemental Zn results in the lowest quantum yield compared to that of Zn carboxylates. This is in agreement with previous studies regarding the demonstration of the enhanced properties of the emission of the InP-based QDs with the use of Zn salts. We showed that the fwhm, however, was not influenced much by the type of Zn precursor involved. The color tunability was observed in the range of 506 to 525 nm with changing the Zn precursor. Regarding the quantum yield, the best performing precursor was found to be zinc stearate, a commonly used Zn carboxylate in the synthesis of InP-based quantum dots. Apart from being employed as the Zn source for alloying the InP core and during the shelling process, Zn precursors were employed to passivate the surface states of the InP-based QDs.

The evolution of the peak emission wavelength and the change in quantum efficiency was plotted in Figure 2, and the

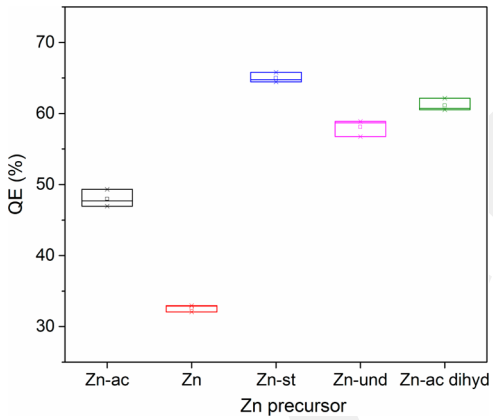

Figure 2. Evolution of the quantum yield of QDs using different Zn precursors.

data for the photoluminescence peak emission wavelength, quantum efficiency, absorbance first excitonic peak, and full width half-maximum value of In(Zn)P/ZnS quantum dots are given in Table 1.

As Zn stearate was found to be the most optimal source of Zn precursor for our synthesis, we investigated the effect of the concentration of Zn stearate at the alloyed core growth stage. In this set of arrangements, we kept all of the concentrations and parameters to be the same during the synthesis (In: 0.12 mmol; myristic acid: 0.36 mmol; 1-dodecanethiol: 0.025 mmol; tris(trimethylsilyl)phosphine: 0.08 mmol) and modified the ratio of the Zn stearate concentration used in the synthesis. We found that increasing the concentration of Zn during the alloyed core growth stage results in significant enhancement of the quantum yield up to 87% after ZnS shell growth. We attributed the increase in the photoluminescence quantum yield to the passivation of the surface defects by using an excessive amount of Zn salt. However, although quantum yield increases with increasing the amount of the Zn precursor used, the yield of the synthesis does not increase accordingly. The synthesis byproducts increase with higher concentrations of the Zn precursor.

Park et al. recently reported 85% photoluminescence yield with InP/GaP/ZnS with fwhm reaching 41 nm.[18] Our result is one of the best reported with such a type of quantum dots of In(Zn)P/ZnS with 55 nm of fwhm using a single ZnS shell coating. Further overcoating the alloyed core−shell particles, we calculated the quantum yield increasing to 88% and emission bandwidth reducing to 50 nm (see the Supporting Information). Figure 3 shows the evolution of the quantum

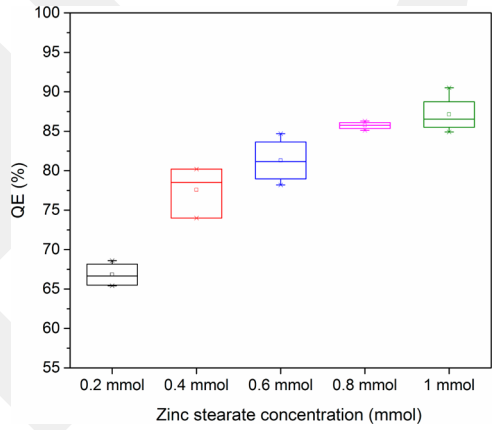

Figure 3. Evolution of quantum yield as a function of Zn stearate concentration.

yield with changing the Zn amount used in the synthesis, and Table 2 presents the optical properties of the synthesized QDs with changing the amount of the Zn precursor from 0.2 to 1.0 mmol.

As for the red emitting QDs, our target is to achieve an efficient FRET acceptor with narrow fwhm, preventing emission cross talk with the green emitter. In the synthesis work, we modified the method in the literature,[19] and by

Table 1. Zn Precursor, Photoluminescence Peak Emission Wavelength, Quantum Efficiency (Mean), Absorbance at First Excitonic Peak and Full Width at Half-Maximum (Mean) of In(Zn)P/ZnS Quantum Dots

Zn precursor	photoluminescence λ_{max} (nm)	quantum efficiency (%)	absorbance peak value (nm)	fwhm (nm)
zinc acetate	506	48	466	43
zinc	511	32	472	46
zinc stearate	521	65	483	47
zinc undecylenate	524	58	485	46
zinc acetate dihydrate	525	61	486	47

Table 2. Photoluminescence Peak Emission Wavelength, Quantum Efficiency (Mean), Absorbance at First Excitonic Peak, and Full Width at Half-Maximum (Mean) of In(Zn)P/ZnS Quantum Dots with Changing Zn Stearate Concentrations

zinc stearate amount (mmol)	photoluminescence λ_{max} (nm)	quantum efficiency (%)	absorbance peak value (nm)	fwhm (nm)
0.2	516	67	474	48
0.4	515	77	475	47
0.6	525	81	482	55
0.8	517	86	474	56
1	515	87	471	54

DOI: 10.1021/acs.jpcc.6b09978
J. Phys. Chem. C 2017, 121, 3034−3043

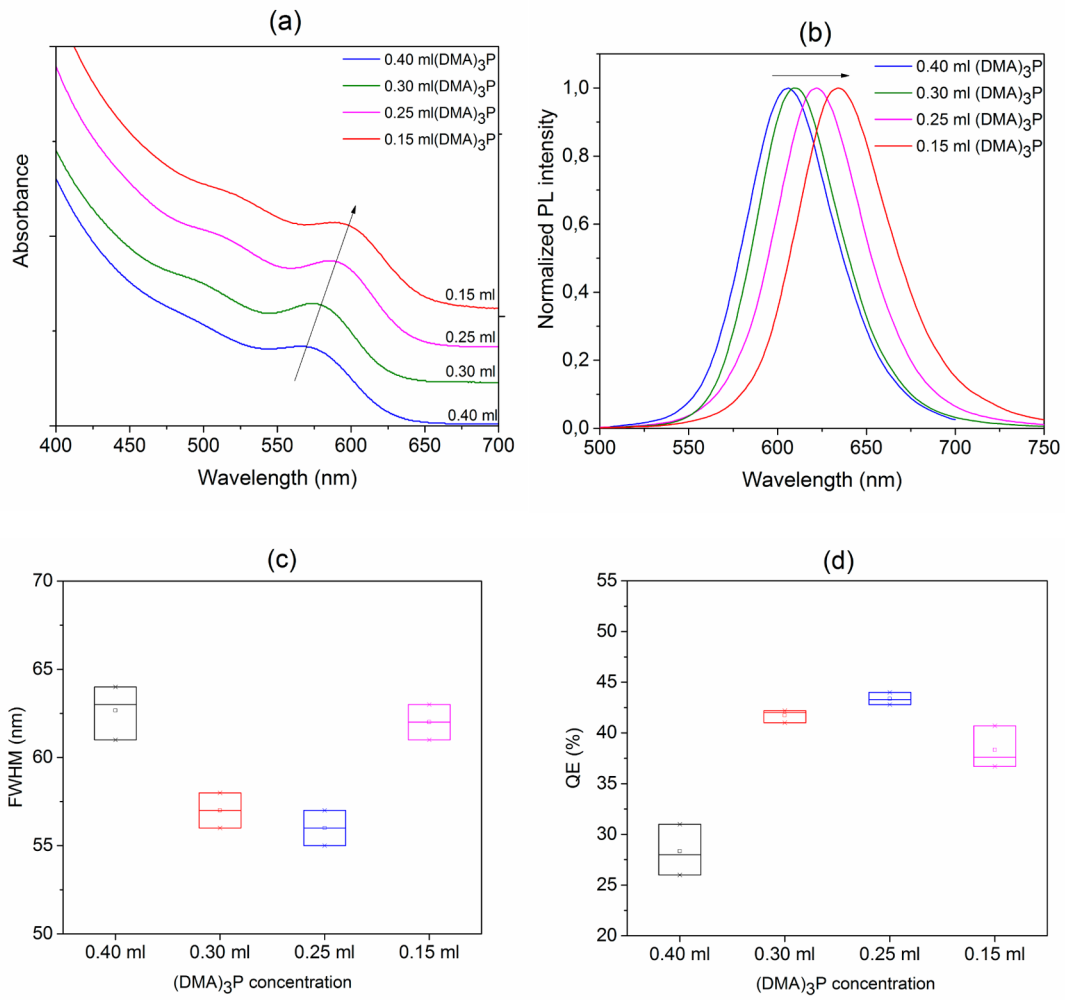

Figure 4. (a) Absorbance, (b) emission, (c) FHWM, and (d) quantum yield evolution of QDs with the changing $(DMA)_3P$ concentration.

changing the concentration of the dimethylamino phosphine, $(DMA)_3P$, we tuned the emission properties of the red emitters. Figures 4a and b present the absorption and emission profiles of the particles, whereas Figures 4c and d show the fwhm and quantum efficiency of colloidal particles as a function of concentration of the P precursor. We showed that decreasing the concentration of the $(DMA)_3P$ red-shifts the emission, enhances the quantum yield of the synthesized QDs, and possesses narrow emitters with 56 nm fwhm. The enhancement of the quantum yield from 29 to 43% and narrowing the fwhm from 63 to 56 nm with decreasing the P precursor ratio has been attributed to the generation of indium-rich surfaces which provided better protection against defect states. However, decreasing the $(DMA)_3P$ concentration further resulted in decreased quantum yield and increased fwhm, which is attributed to the P precursor not being sufficient enough to provide defect-free particles. The optical properties are further presented in Table 3 for the red emitting QDs.

To investigate the nonradiative energy transfer between the green and red emitters, we studied the formation of the polymeric films of quantum dots by blending them with poly(methyl methacrylate) (PMMA) (18% in anisole) overnight and drop casting them on glass slides. We prepared samples with different ratios of the green and red emitters as in the following: red:green with 0.25*x*:0, 0.25*x*:1.00*y*, 0.50*x*:0, 0.50*x*:1.00*y*, 1.00*x*:0, 1.00*x*:1.00*y*, 2.00*x*:0, 2.00*x*:1.00*y*, and 0:*y*.

Table 3. Photoluminescence Peak Emission Wavelength, Quantum Efficiency (Mean), Absorbance at First Excitonic Peak, and Full Width at Half-Maximum (Mean) of Red Emitting Quantum Dots with the Changing Amount of $(DMA)_3P$

$(DMA)_3P$ used (mL)	quantum efficiency (%)	photoluminescence $\lambda_{max\ (nm)}$	absorbance peak value (nm)	fwhm (nm)
0.40	29	605	566	63
0.30	42	615	577	57
0.25	43	624	587	56
0.15	38	634	591	62

Here, *x* and *y* correspond to the number of acceptor and donor particles in the film, respectively, calculated as *x*:*y* (1.91×10^{15}:1.29×10^{15}). In this set of samples, we were able to study the effect of the emission kinetics of the acceptor in the presence of donor and the emission kinetics of the donor in the presence of acceptor together with the control groups of donor-only and acceptor-only samples. Figure 5a demonstrates the in-solution photoluminescence and absorption spectra for the chosen FRET pair. Figure 5b shows the photoluminescence excitation (PLE) spectra, which resemble the absorbance curves. The emission kinetics, i.e., the time-correlated single photon counting decays of the emitters, is presented in Figure 5c. Figures 5d and e show the images of the green and red

DOI: 10.1021/acs.jpcc.6b09978
J. Phys. Chem. C 2017, 121, 3034−3043

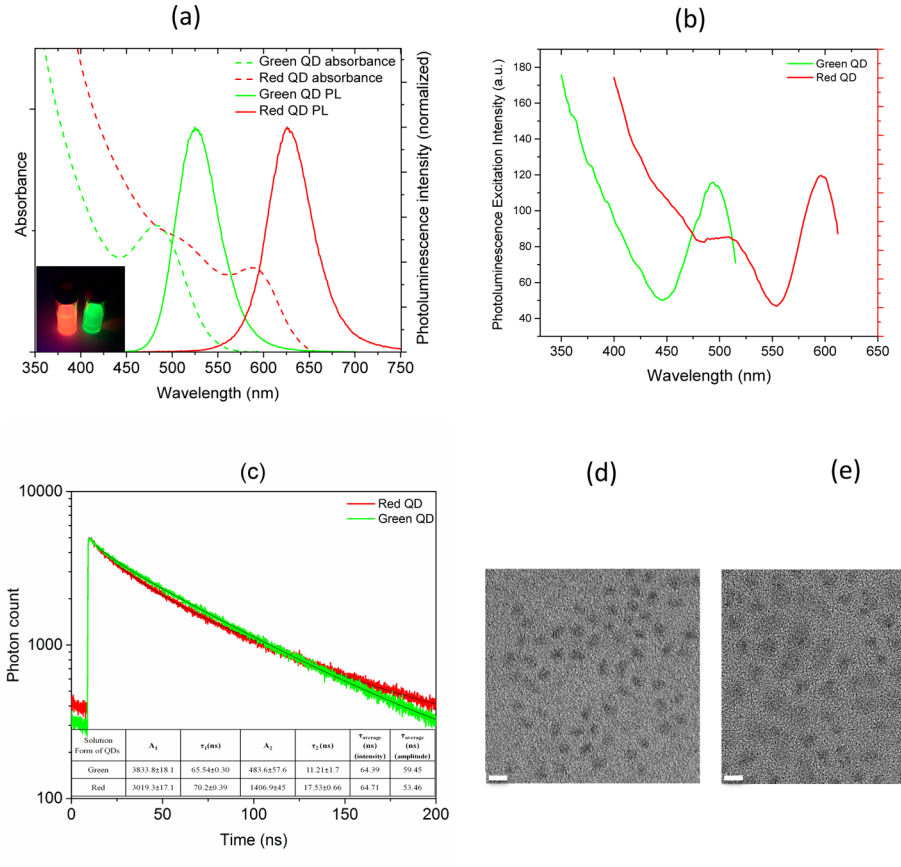

Figure 5. (a) Absorbance and photoluminescence spectra; (b) photoluminescence excitation spectra of the green and red emitting QDs; (c) time-correlated single photon counting decays of green and red emitting QDs along with their lifetime coefficients, lifetime components, and intensity-weighted and amplitude-weighted lifetimes; (d) high-resolution transmission electron microscopy image of green QDs; and (e) high-resolution transmission electron microscopy image of red QDs (scale bar is 5 nm).

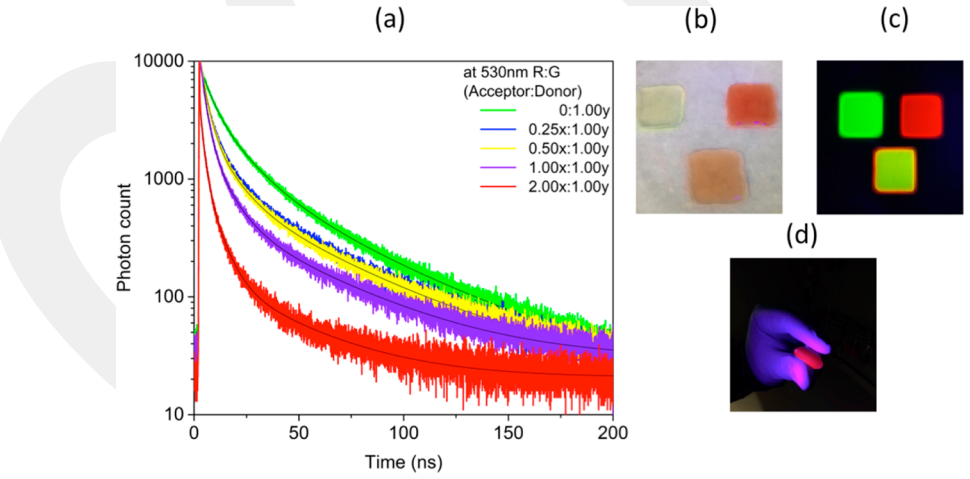

Figure 6. (a) Time-correlated single photon counting decays of FRET mediated system with green and red emitting QDs changing their ratio in film (at donor peak emission wavelength). (b) Photograph of bare donor, bare acceptor, and mixed film under daylight. (c) Photograph of bare donor, bare acceptor, and mixed film under UV illumination. (c) Photograph of the flexible red emitting film under UV illumination.

quantum dots using high-resolution transmission electron microscopy.

During the measurements of time-correlated single photon counting, a 375 nm emitting diode laser was used as the pump source with tunable repetition range to cover the whole decay of the emitter (using PicoQuant FluoTime 200 system equipped with Time Harp 260). The lifetime of the green emitter was calculated as 59.45 ns, whereas the red emitter lifetime was 53.46 ns when fit with 2 exponentials (in solution). The amplitude-weighted lifetime is given as

$$\tau_{amp} = \frac{A_1\tau_1 + A_2\tau_2}{A_1 + A_2} \quad (1)$$

and the intensity-weighted lifetime is given as

DOI: 10.1021/acs.jpcc.6b09978
J. Phys. Chem. C 2017, 121, 3034−3043

Table 4. Amplitudes, Lifetime Components, and Amplitude-Weighted Lifetimes for Acceptor:Donor Pairs (at Donor Emission Wavelength)

red:green (acceptor:donor)	A_1	τ_1 (ns)	A_2	τ_2 (ns)	A_3	τ_3 (ns)	$\tau_{average}$ (ns) (amplitude)
0:1.00*y*	1179.1 ± 14.9	48.37 ± 0.43	3329.2 ± 50.1	14.78 ± 0.19	4080 ± 112	5.05 ± 0.15	14.77
0.25*x*:1.00*y*	867.1 ± 12.6	44.75 ± 0.50	2490.7 ± 56.1	9.851 ± 0.20	4709 ± 140	2.97 ± 0.1	9.58
0.50*x*:1.00*y*	756 ± 11.8	45.47 ± 0.55	1987.5 ± 49.4	10.54 ± 0.23	4403 ± 128	3.07 ± 0.1	9.63
1.00*x*:1.00*y*	471.9 ± 9.86	43.99 ± 0.72	1702.5 ± 48	8.89 ± 0.22	4048 ± 126	2.63 ± 0.1	7.48
2.00*x*:1.00*y*	139.58 ± 6.58	36.93 ± 1.42	1065.8 ± 40.4	6.32 ± 0.19	2480 ± 117	1.74 ± 0.1	4.39

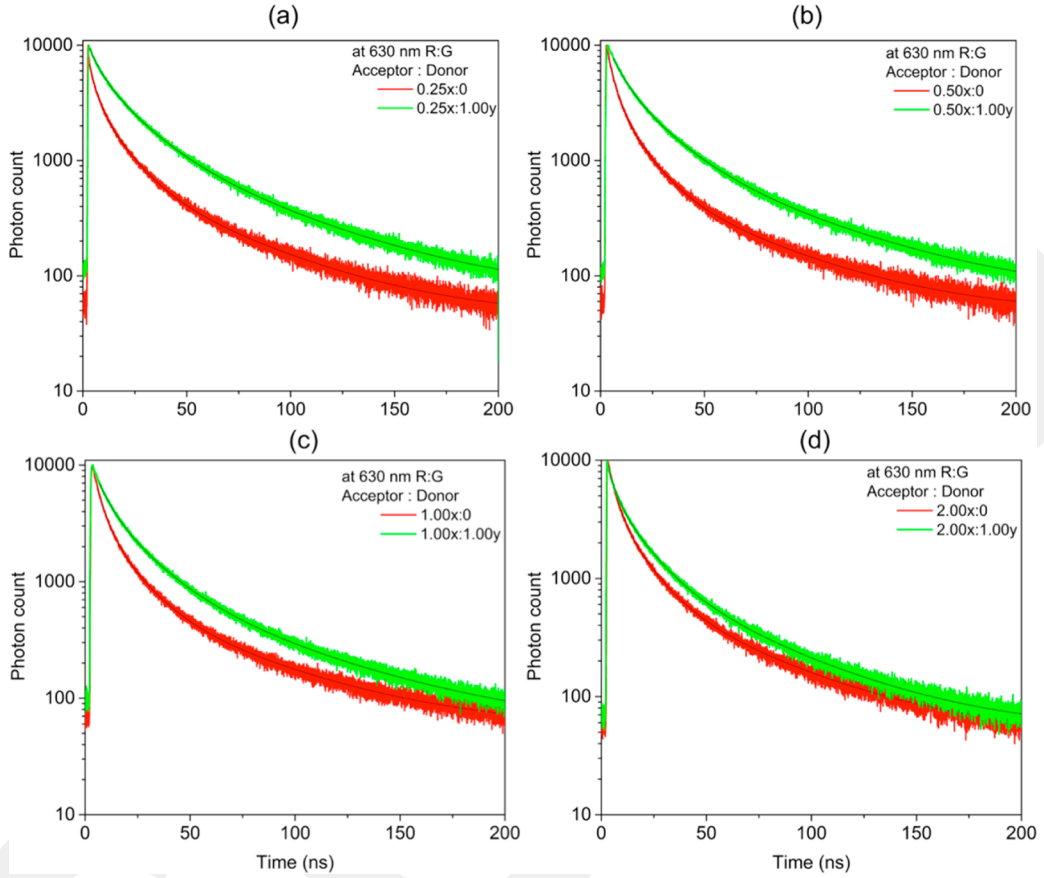

Figure 7. Time-correlated single photon counting decays of FRET mediated system with green and red emitting QDs changing their ratio in film with red to green ratios of (a) 0.25*x*:0 and 0.25*x*:1.00*y*, (b) 0.50*x*:0 and 0.50*x*:1.00*y*, (c) 1.00*x*:0 and 1.00*x*:1.00*y*, and (d) 2.00*x*:0 and 2.00*x*:1.00*y* (at acceptor peak emission wavelength).

$$\tau_{int} = \frac{A_1\tau_1^2 + A_2\tau_2^2}{A_1\tau_1 + A_2\tau_2} \quad (2)$$

For the investigation of FRET, we carried out our discussions through the amplitude-weighted lifetimes rather than the intensity-weighted lifetime.[20]

We investigated the effect of acceptor on the emission kinetics of the donor QDs. Figure 6 presents the time-resolved decays of the donor control group (0:1.00*y*) with increasing the acceptor in the film sample (analyzed at peak donor emission wavelength). Fittedwith the 3 exponentials, the amplitude-weighted lifetime of the green-only QD containing sample was found to be 14.77 ns. When the acceptor QDs were introduced to the medium, the lifetime of the donor decreases to 9.58 ns in the case of 0.25*x*:1.00*y*, to 9.63 ns in the case of 0.50*x*:1.00*y*, to 7.48 ns in the case of 1.00*x*:1.00*y*, and to 4.39 ns in the case of 2.00*x*:1.00*y* (Table 4). Observation of a faster decay for the case of the donor is expected as the green emitter is employed as the energy-transferring agent. The lifetime components become shorter as more and more acceptors per donor are introduced to the medium.

One can calculate the FRET efficiency from the following equation

$$\eta = 1 - \frac{\tau_{DA}}{\tau_D} \quad (3)$$

where τ_{DA} is the lifetime of the donor in the presence of the acceptor and τ_D is the lifetime of the donor in the absence of the acceptor. From the observed lifetimes, the FRET efficiency has been calculated as 70.3% at the maximum level.

To see the effect of donor QDs on the acceptor QD lifetime, we analyzed the lifetime of the acceptor at its peak emission wavelength. In this analysis, we monitored the lifetime of the acceptor sample with and without donor in the proximity. The characterizations were performed at four different concentration regimes with increasing the acceptor amount while keeping the donor amount the same. In that regard, we systematically increased the acceptor amount by the same

DOI: 10.1021/acs.jpcc.6b09978
J. Phys. Chem. C 2017, 121, 3034−3043

Table 5. Amplitudes, Lifetime Components, and Amplitude-Weighted Lifetimes for Green and Red QDs (at Acceptor Emission Wavelength)

red:green (acceptor:donor)	A_1	τ_1 (ns)	A_2	τ_2 (ns)	A_3	τ_3 (ns)	$\tau_{average}$ (ns) (amplitude)
0.25*x*:0	774.3 ± 12.6	49.27 ± 0.61	2913.3 ± 48.5	12.32 ± 0.19	3076 ± 132	3.05 ± 0.15	12.34
0.25*x*:1.00*y*	1689.6 ± 17.8	54.77 ± 0.45	4820.3 ± 55.4	16.63 ± 0.18	2841 ± 133	4.65 ± 0.26	19.88
0.50*x*:0	699.5 ± 12.1	49.56 ± 0.65	3070.1 ± 50.5	11.96 ± 0.17	4190 ± 135	3.24 ± 0.12	10.68
0.50*x*:1.00*y*	1300 ± 14.9	58.24 ± 0.50	3864 ± 46.1	17.9 ± 0.20	2501 ± 101	5.84 ± 0.28	20.81
1.00*x*:0	678.4 ± 11.3	54.39 ± 0.69	2681.9 ± 44	13.56 ± 0.20	3267 ± 111	3.88 ± 0.15	12.97
1.00*x*:1.00*y*	1041 ± 13.4	60.30 ± 0.59	3467.5 ± 43.3	17.85 ± 0.20	2457.3 ± 97.2	5.69 ± 0.26	19.91
2.00*x*:0	811.8 ± 13.1	48.56 ± 0.59	3523.5 ± 53.3	12.17 ± 0.16	4642 ± 142	3.30 ± 0.11	10.87
2.00*x*:1.00*y*	1148.5 ± 15.2	48.74 ± 0.45	3878.8 ± 52.4	13.74 ± 0.17	3165 ± 130	3.81 ± 0.18	14.81

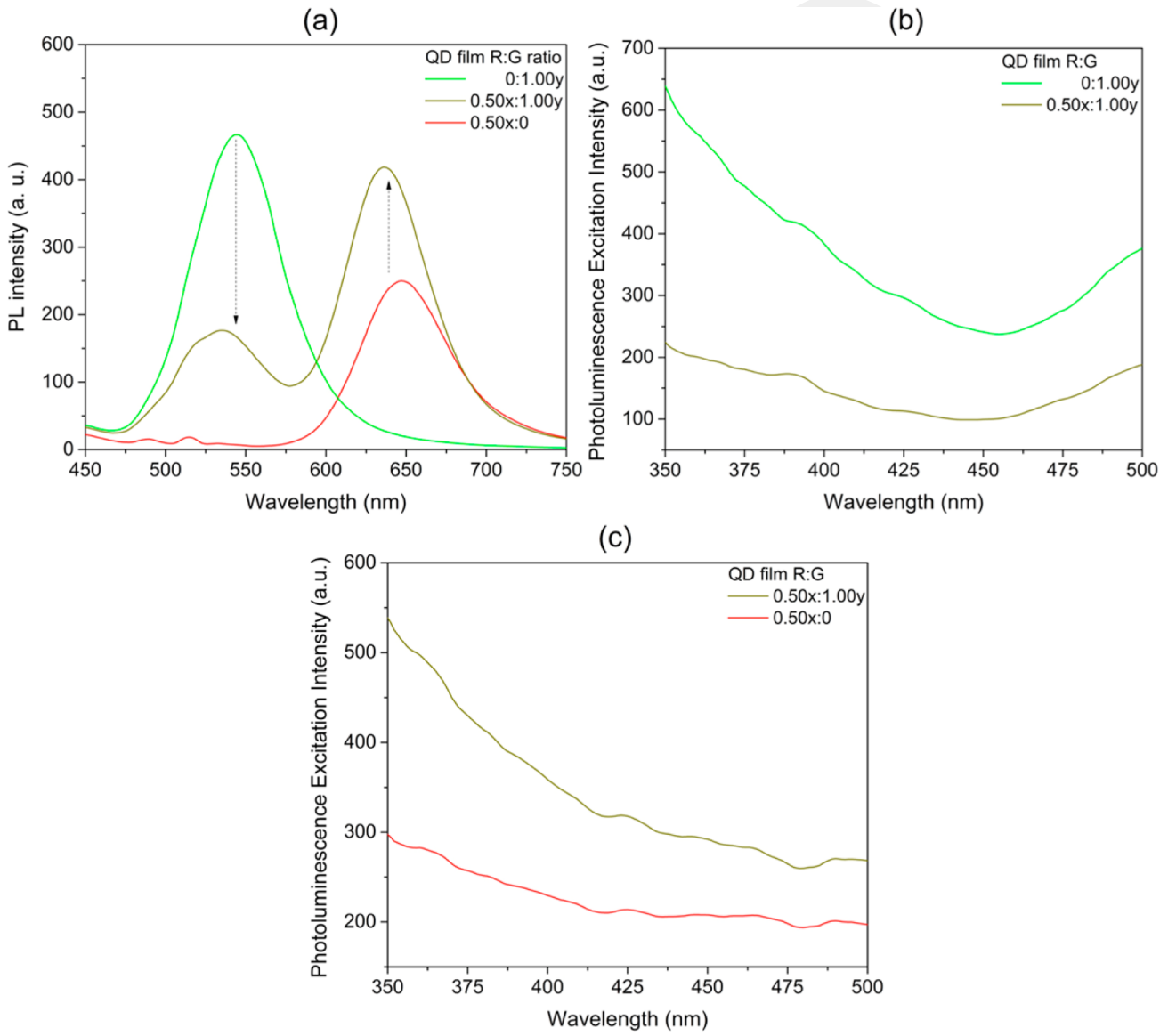

Figure 8. (a) Steady state photoluminescence enhancement of the mixed film of green and red emitters. (b) Photoluminescence excitation spectra of the bare green and mixed film (at green peak emission). (c) Photoluminescence excitation spectra of the bare red and mixed film (at red peak emission.

amount of donor in the film together with their control groups. Figure 7 presents the lifetime decays, monitored at the acceptor emission peak wavelength for different concentrations of acceptor in the medium. As a result of FRET, one expects an increase in the lifetime of the acceptor as a result of energy feeding. However, because the donor amount is the same in the medium, the increase in the acceptor lifetime by introducing donor QDs reduces (Figures 7c and d). This is due to the fact that, from the low- to high-concentration limit of the acceptor, there are less and less donor molecules for each acceptor, which limits the energy transfer. Expressed in terms of the acceptor lifetimes, at a red to green ratio of 1.00*x*:1.00*y*, compared with

DOI: 10.1021/acs.jpcc.6b09978
J. Phys. Chem. C 2017, 121, 3034−3043

the bare acceptor only, the acceptor lifetime increases from 12.97 to 19.91 ns. This is also visible from the energy feeding observation in the first few nanoseconds of the decay. As the acceptor concentration is further increased to a ratio level of red:green 2.00*x*:1.00*y*, the bare acceptor lifetime increases from 10.87 to 14.81 ns.

It is worth noting here that at the low-concentration regime, although less acceptors per donor is expected to have a high energy feeding observed from the lifetime, the other consideration is the interparticle distance. Therefore, we observed that reducing the red:green ratio further to 0.25*x*:1.00*y* does not possess large energy feeding to the acceptor (Figure 7a). Therefore, there is a trade off observed with less acceptors per donor favoring the energy feeding to the acceptor; however, because particle to particle distance is now reduced, the effect is hindered. In our experiments, the maximum energy feeding to the acceptor from the donor is observed in the case of the red:green ratio of 0.50*x*:1.00*y*, which corresponds to the lifetime modification of 10.68 to 20.81 ns. In that experimental set, the donor−acceptor distance was determined as 3.10 nm, whereas the Förster radius is calculated as 5.95 nm. The details of the calculation of the Förster radius and extinction coefficients are given in the Methods section.

The results of the lifetime analysis are summarized in Table 5 along with the amplitude and lifetime components.

Furthermore, we carried out a steady state photoluminescence measurement for the acceptor and donor pair with a predetermined ratio of red:green of 0.50*x*:1.00*y*. Considering the control groups of bare donor (red:green 0:1.00*y*) and bare acceptor (red:green 0.50*x*:0), upon excitation with 375 nm monochromatic light, we saw that the intensity of the red enhances 63% when prepared in a film structure together with the donor green emitting species. On the other hand, due to energy transfer, the intensity of the green emitting QDs quenches to 34% of its initial intensity (Figure 8a). To reveal the origin of the photoluminescence enhancement, we carried out PLE measurements of the donor-only, acceptor-only, and mixed film. Figure 8b demonstrates the PLE signal intensity modification for the donor quantum dot, and Figure 8c shows the PLE signal intensity modification for the acceptor quantum dot. In the low-wavelength regime, the PLE signal possesses around twofold enhancement, considering the PLE enhancement at 350 nm excitation wavelength (when the monochromator is set at the red emission peak) and is in agreement with the observed enhancement in steady state photoluminescence. The observed decrease in the PLE signal enhancement in the longer wavelength regime (for the acceptor QDs) is attributed to the reduced absorption coefficient of the quantum dot in that spectral window.

CONCLUSIONS

In conclusion, we extensively investigated the effect of the Zn precursor on the quality of the In(ZnP) quantum dots. The type of the Zn precursor and its concentration was studied, and we achieved up to 87% quantum yield for the green emitting colloidal quantum dots. The green emitting donor quantum dots were mixed with red emitting acceptor quantum dots, and Förster-type nonradiative energy transfer was investigated between the QD−QD pairs. We demonstrated and discussed the effect of donor and acceptor in the presence and absence of the individual and their influence on emission kinetics. Our results indicated up to 70.3% FRET efficiency between green and red emitting InP-based quantum dots. Furthermore, we showed enhancement of the acceptor photoluminescence intensity upon FRET. These efforts on the investigation of the high- efficiency, narrow-bandwidth, environmentally friendly component-based colloidal particles and the study of the excitonic interaction among them will open up new areas for further research on the subject.

METHODS

All mentioned chemicals were purchased from Sigma-Aldrich and used without further purification.

Synthesis of Green Emitting QDs. Following the modified methods outlined in previous works,[4,5,17] indium acetate (0.12 mmol), myristic acid (0.36 mmol), and 6 mL of octadecene were added in the three necked flask, heated to 100 °C, and kept under vacuum for 1 h. The solution was cooled to room temperature, and then zinc stearate purum (0.1 mmol) (or other Zn sources used) and 1-dodecanethiol (0.025 mmol) were added, and the flask was heated to 220 °C under argon atmosphere and stirring. After that, the solution of tris(trimethylsilyl)phosphine (0.08 mmol in 1 mL of octadecene) was swiftly injected into the hot solution at 220 °C, and then the temperature was increased to 285 °C for 10 min. When the synthesis finished, the solution was cooled to room temperature.

For the shell coating process, zinc stearate purum (0.2 mmol) (or other Zn sources used) was added to the reaction flask at room temperature, and the solution was heated to 230 °C for 3 h. After that, the solution of 1-dodecanethiol (0.4 mmol in 1 mL of octadecene) was injected drop by drop into the flask and kept for 1 h. When the shell synthesis process was finished, the solution was cooled to room temperature. First, the precipitate, including unreacted species of ligands and other precursors, was removed with 5 mL of hexane at 5000 rpm for 10 min. Second, the supernatant solution was precipitated with 20 mL of acetone and 3 mL of methanol, and then it was centrifuged twice at 5000 rpm for 10 min. The particles were redissolved in hexane. The green emitting particles with highest QE were achieved by using 1 mmol Zn-stearate as the Zn precursor during the core process followed by shell growth.

Synthesis of Red Emitting QDs. For the synthesis of highly efficient red emitting InP/ZnS QDs, the reported method outlined previously in the literature[19] was modified using tris(dimethylamino)phosphine instead of tris(diethylamino)phosphine and modifying the purity of the precursors and other conditions. The InP/ZnS QDs were prepared by the hot injection method on a Schlenk line with a standard air-free route. All chemicals were used without further purification.

Following a similar recipe with the work of Tessier et.al.,[19] $InCl_3$ (99%, 0.45 mmol), $ZnCl_2$ (98%, 2.2 mmol), and 5 mL of oleylamine (technical grade, 15 mmol) were added in the round-bottom flask and stirred at room temperature for 5 min under vacuum and Ar gas sequentially. The temperature was then increased to 120 °C under 800 rpm stirring for 1 h under vacuum. After that, the solution was heated to 180 °C under an Ar gas flow. When the temperature reached 180 °C, 250 μL of tris(dimethylamino)phosphine (prepared in a glovebox) was injected, and the reaction was allowed to proceed for 20 min with strong agitation continuously. After 20 min, the reaction was continued for the shell process without cooling of the reacting mixture to room temperature.

Initially, a stock solution of sulfur in trioctylphosphine (TOP-S) was prepared in the glovebox with the concentration

DOI: 10.1021/acs.jpcc.6b09978
J. Phys. Chem. C 2017, 121, 3034−3043

of S (0.72 g) into TOP (10 mL), and a stock solution of zinc stearate (Zn st, purum) in 1-octadecene (1-ODE, 90%) was prepared by dissolving zinc stearate purum (4.5 g) into 1-ODE (20 mL) under an Ar gas atmosphere at 180 °C in a 50 mL three-necked flask. 1 milliliter of stock solution of TOP-S was injected in the solution of InP QDs at 180 °C for 40 min (total reaction time = 60 min). The solution was then heated from 180 to 200 °C, and the reaction was allowed to proceed for 1 h (total reaction time = 120 min). Later, 4 mL of zinc stearate−octadecene (ODE) stock solution was added slowly into the mixture, and the temperature was increased from 200 to 220 °C and kept there for 30 min (total reaction time = 150 min). Then, 0.7 mL of TOP-S solution was injected slowly, and the flask was heated from 220 to 240 °C for 30 min (total reaction time = 180 min). 2 milliliters of zinc stearate−ODE stock solution was slowly injected into the reaction mixture at 240 °C and heated to 260 °C for 30 min (total reaction time = 210 min). Finally, the reaction was stopped at 210 min, and flask was allowed to cool to room temperature for final purification of synthesized QDs. The final product was transferred into centrifuge tubes and washed with hexane twice at 5000 rpm for 5 min each to eliminate any solid unreactive byproducts. The supernatant solution was washed using acetone and methanol for 20 min at 5000 rpm, and the final QDs were dispersed in hexane/chloroform for further characterization and use.

The quantum efficiency was calculated by comparing the emission intensity of the QDs with organic dye rhodamine 6G (for green emitters) and sulforhodamine (for red emitters) with quantum efficiency of 95% and 90% in absolute ethanol, respectively, using the eq 4.[21]

$$\mathrm{QE}_{\mathrm{sample}} = \mathrm{QE}_{\mathrm{ref.dye}} \frac{I_{\mathrm{sample}}}{I_{\mathrm{ref.dye}}} \left(\frac{n_{\mathrm{sample}}}{n_{\mathrm{ref.dye}}} \right)^2 \tag{4}$$

Here, I represents the integrated photoluminescence intensity when the reference dye and sample has been excited at the same excitation wavelength (extracted from the intersection point at the absorbance curves). When the quantum yield was measured, the concentration of the solutions were adjusted to not exceed 0.1−0.2 to prevent reabsorption, and excitation wavelengths (thus the absorbance intersection) were chosen to be in the appropriate range for excitation of the reference dyes to prevent misleading interpretation.

Calculation of the Extinction Coefficient and Förster Radius. The Förster radius is given by

$$R_0 = 0.211(\kappa^2 n^{-4} Q_D J(\lambda))^{1/6} \tag{5}$$

where κ^2 is the orientation factor (taken as 2/3 for random orientation), n is the refractive index of the media (1.496 for poly(methyl methacrylate)), Q_D is the quantum efficiency of the donor (taken as 10% in film), and $J(\lambda)$ is the overlap integral given by

$$J(\lambda) = \int_0^\infty I_D(\lambda)\varepsilon_A(\lambda)\lambda^4 d\lambda \tag{6}$$

where $I_D(\lambda)$ is the normalized integrated emission spectrum of the donor and $\varepsilon_A(\lambda)$ is the wavelength-dependent extinction coefficient of the acceptor (calculated as 1.05×10^6 and 4.14×10^6 for green and red emitters, respectively, using $\varepsilon_{335} = (4.40 \pm 0.19) \times 10^4\ d{Q_D^3}$).[22] The average diameters of the QDs were determined to be 2.88 nm for green and 4.55 nm for red emitting ones, extracted from the TEM measurement by averaging through the ensemble of the particles. When the calculations to determine the Förster radius were followed, it was found to be 5.95 nm.

Further calculation (for the ratio of red to green intensity ratio of 1.00x:0.50y) to estimate the particle-to-particle distance was carried out using the volume analysis. Starting with the volume of the film ($5.32 \times 10^{-8}\mathrm{m}^3$) (the size of the film is measured to be $2.2 \times 2.2 \times 0.011$ cm), the volume per particle ($2.38 \times 10^{-25}\ \mathrm{m}^{-3}$) yields an approximated distance of 3.10 nm between quantum dots. When the ligands attached to the quantum dots and approximations are considered, the order of magnitude of interparticle distance is in acceptable agreement with the calculated Förster radius.

Characterizations. Photoluminescence characterizations and UV−vis spectroscopy were performed using an Agilent-Cary Eclipse fluorescence spectrophotometer and a UV−vis Thermo Genesys 10S spectrometer, respectively. Time-correlated single photon counting measurements were carried out using a Pico Quant FluoTime 200 equipped with a 375 nm pulsed laser diode. TEM images were taken using an FEI Tecnai G2 F30; energy-dispersive X-ray (EDX) measurements were collected during the TEM imaging, and X-ray photoelectron spectroscopy (XPS) measurements were conducted using a Thermo Scientific Kα X-ray photoelectron spectrometer system. Dynamic light scattering measurements were performed using a Malvern Zeta Sizer.

■ ASSOCIATED CONTENT

Supporting Information

The Supporting Information is available free of charge on the ACS Publications website at DOI: 10.1021/acs.jpcc.6b09978.

TCSPC spectrum and lifetime analysis for the investigation of the effect of multishell coatings on the green QDs (0.5 mmol Zn stearate), TEM and EDX analysis of quantum dots synthesized, particle size measurements for red and green emitting QDs, XPS measurements for green and red emitting QDs in a polymer matrix, and a photograph of FRET samples under UV illumination (PDF)

■ AUTHOR INFORMATION

Corresponding Author

*E-mail: evren.mutlugun@agu.edu.tr; Phone: +90-352-2248800.

ORCID

Evren Mutlugün: 0000-0003-3715-5594

Notes

The authors declare no competing financial interest.

■ ACKNOWLEDGMENTS

The authors would like to thank financial support from the TUBITAK 114E107, 5140079, and BAGEP 2014 awards. M.Y.T. acknowledges support from the TUBITAK 2221 fellowship program. The authors further acknowledge Yusuf Kelestemur at Bilkent University for his assistance on TEM characterizations.

■ REFERENCES

(1) Talapin, D. V.; Shevchenko, E. V. Introduction: Nanoparticle Chemistry. *Chem. Rev.* **2016**, *116*, 10343−10345.

DOI: 10.1021/acs.jpcc.6b09978
J. Phys. Chem. C 2017, 121, 3034−3043

(2) Grim, J. Q.; Manna, L.; Moreels, I. A. Sustainable Future For Photonic Colloidal Nanocrystals. *Chem. Soc. Rev.* **2015**, *44*, 5897−5914.
(3) Battaglia, D.; Peng, X. Formation of High Quality InP and InAs Nanocrystals in a Noncoordinating Solvent. *Nano Lett.* **2002**, *2*, 1027−1030.
(4) Kim, T.; Kim, S. W.; Kang, M.; Kim, S- W. Large-Scale Synthesis of InPZnS Alloy Quantum Dots with Dodecanethiol as a Composition Controller. *J. Phys. Chem. Lett.* **2012**, *3*, 214−218.
(5) Altıntas, Y.; Talpur, M. Y.; Ünlü, M.; Mutlugün, E. Highly Efficient Cd-Free Alloyed Core/Shell Quantum Dots with Optimized Precursor Concentrations. *J. Phys. Chem. C* **2016**, *120*, 7885−7892.
(6) Nightingale, A. M.; deMello, J. C. Improving The Ensemble Optical Properties Of InP Quantum Dots By Indium Precursor Modification. *J. Mater. Chem. C* **2016**, *4*, 8454−8458.
(7) Ramasamy, P.; Kim, B.; Lee, M.-S.; Lee, J.-S. Beneficial Effects Of Water In The Colloidal Synthesis Of InP/ZnS Core−Shell Quantum Dots For Optoelectronic Applications. *Nanoscale* **2016**, *8*, 17159−17168.
(8) Xi, L.; Cho, D.-Y.; Duchamp, M.; Boothroyd, C. B.; Lek, J. Y.; Besmehn, A.; Waser, R.; Lam, Y. M.; Kardynal, B. Understanding the Role of Single Molecular ZnS Precursors in the Synthesis of In(Zn)P/ZnS Nanocrystals. *ACS Appl. Mater. Interfaces* **2014**, *6*, 18233−18242.
(9) Xi, L.; Cho, D.-Y.; Besmehn, A.; Duchamp, M.; Grützmacher, D.; Lam, Y. M.; Kardynal, B. E. Effect of Zinc Incorporation on the Performance of Red Light Emitting InP Core Nanocrystals. *Inorg. Chem.* **2016**, *55*, 8381−8386.
(10) Harris, D. K.; Bawendi, M. G. Improved Precursor Chemistry for the Synthesis of III−V Quantum Dots. *J. Am. Chem. Soc.* **2012**, *134*, 20211−20213.
(11) Yang, X.; Zhao, D.; Leck, K. S.; Tan, S. T.; Tang, Y. X.; Zhao, J.; Demir, H. V.; Sun, X. W. Full Visible Range Covering InP/ZnS Nanocrystals with High Photometric Performance and Their Application to White Quantum Dot Light-Emitting Diodes. *Adv. Mater.* **2012**, *24*, 4180−4185.
(12) Lim, J.; Park, M.; Bae, W. K.; Lee, D.; Lee, S.; Char, K. Highly Efficient Cadmium-Free Quantum Dot Light-Emitting Diodes Enabled by the Direct Formation of Excitons within InP@ZnSeS Quantum Dots. *ACS Nano* **2013**, *7*, 9019−9026.
(13) Mutlugun, E.; Samarskaya, O.; Ozel, T.; Cicek, N.; Gaponik, N.; Eychmüller, A.; Demir, H. V. Highly Efficient Nonradiative Energy Transfer Mediated Light Harvesting in Water Using Aqueous CdTe Quantum Dot Antennas. *Opt. Express* **2010**, *18*, 10720−10730.
(14) Mutlugun, E.; Martinez, P. L. H.; Eroglu, C.; Coskun, Y.; Erdem, T.; Sharma, V. K.; Unal, E.; Panda, S. K.; Hickey, S. G.; Gaponik, N.; et al. Large-area (over 50 cm × 50 cm) Freestanding Films of Colloidal InP/ZnS Quantum Dots. *Nano Lett.* **2012**, *12*, 3986−3993.
(15) Thomas, A.; Nair, P. V.; Thomas, K. G. InP Quantum Dots: An Environmentally Friendly Material with Resonance Energy Transfer Requisites. *J. Phys. Chem. C* **2014**, *118*, 3838−3845.
(16) Guzelturk, B.; Demir, V. Near-Field Energy Transfer Using Nanoemitters For Optoelectronics. *Adv. Funct. Mater.* **2016**, *26*, 8158−8177.
(17) Li, L.; Reiss, P. One-Pot Synthesis of Highly Luminescent InP/ZnS Nanocrystals without Precursor Injection. *J. Am. Chem. Soc.* **2008**, *130*, 11588−11589.
(18) Park, J. P.; Lee, J.-J.; Kim, S.-W. Highly Luminescent Inp/Gap/Zns QDs Emitting in the Entire Color Range via a Heating Up Process. *Sci. Rep.* **2016**, *6*, 30094−30099.
(19) Tessier, M. D.; Dupont, D.; De Nolf, K.; De Roo, J.; Hens, Z. Economic and Size-Tunable Synthesis of InP/ ZnE (E = S,Se) Colloidal Quantum Dots. *Chem. Mater.* **2015**, *27*, 4893−4898.
(20) Lakowicz, J. R. *Principles of Fluorescence Spectroscopy*; Springer: New York, 2007.
(21) Crosby, G. A.; Demas, J. N. Measurement of Photoluminescence Quantum Yields. Review. *J. Phys. Chem.* **1971**, *75*, 991−1024.
(22) Ministro, J. *A study on the synthesis and the optical properties of InP-based quantum dots*. M.Sc. Thesis, University of Ghent, Belgium, 2013.

DOI: 10.1021/acs.jpcc.6b09978
J. Phys. Chem. C 2017, 121, 3034−3043